Improved activity of MC3T3-E1 cells by the exciting piezoelectric $BaTiO_3$/TC4 using low-intensity pulsed ultrasound

Kunzhan Cai [a], Yilai Jiao [b], Quan Quan [a], Yulin Hao [b], Jie Liu [c], Lin Wu [a,*]

[a] School and Hospital of Stomatology, China Medical University, Liaoning Provincial Key Laboratory of Oral Diseases, Shenyang, 110001, China
[b] Shenyang National Laboratory for Materials Science, Institute of Metal Research, Chinese Academy of Sciences, Shenyang, 110016, China
[c] Department of Science Experiment Center, China Medical University, Shenyang, 110122, China

ARTICLE INFO

ABSTRACT

Developing bioactive materials for bone implants to enhance bone healing and bone growth has for years been the focus of clinical research. Barium titanate (BT) is an electroactive material that can generate electrical signals in response to applied mechanical forces. In this study, a BT piezoelectric ceramic coating was synthesized on the surface of a TC4 titanium alloy, forming a BT/TC4 material, and low-intensity pulsed ultrasound (LIPUS) was then applied as a mechanical stimulus. The combined effects on the biological responses of MC3T3-E1 cells were investigated. Results of scanning electron microscopy, energy-dispersive X-ray spectroscopy, and X-ray diffraction showed that an uniform nanospheres -shaped BT coating was formed on TC4 substrate. Piezoelectric behaviors were observed using piezoelectric force microscopy with the piezoelectric coefficient d_{33} of 0.42 pC/N. Electrochemical measures indicated that LIPUS-stimulated BT/TC4 materials could produce a microcurrent of approximately 10 $\mu A/cm^2$. *In vitro*, the greatest osteogenesis (cell adhesion, proliferation, and osteogenic differentiation) was found in MC3T3-E1 cells when BT/TC4 was stimulated using LIPUS. Furthermore, the intracellular calcium ion concentration increased in these cells, possibly because opening of the L-type calcium ion channels was promoted and expression of the $Ca_V1.2$ protein was increased. Therefore, the piezoelectric BT/TC4 material with LIPUS loading synergistically promoted osteogenesis, rending it a potential treatment for early stage formation of reliable bone-implant contact.

1. Introduction

The ideal material for implants should possess bioactivity that is similar to that in natural bone, thus encouraging osseointegration and the formation of reliable bone-implant contact. Titanium and its alloys have been widely used in dental and orthopedic implants, given their superior biocompatibility, excellent corrosion resistance, and favorable mechanical properties [1–3]; however, because they are considered bio-inert, they are not anticipated to augment bio-interaction with surrounding tissues [4,5]. To enhance surface bioactivity while retaining desirable inherent characteristics, titanium and its alloys are commonly surface-coated to shorten osseointergration periods [6,7].

It is well established that electric signals play vital roles in bone formation and fracture healing [8]. Natural bone tissues are known to exhibit piezoelectricity [9], therefore, piezoelectric materials are promising in implants because they can convert mechanical forces to electrical signals, giving them the ability to provide electrical stimulation to surrounding bone tissues without surgically implanting electrodes [10,11]. As the first reported piezoelectric ceramic used in bone regeneration research, barium titanate ($BaTiO_3$; BT) has received extensive attention as a lead-free implant material with good biocompatibility [12–14]. Studies have shown that composites containing BT have significant potential as bone substitutes both *in vivo* and *in vitro* [15, 16]. Although existing investigations focus on BT combined with non-metallic substrates, titanium-based materials are the gold standard for large bone implants such as knee and hip replacements, given their close-to-ideal mechanical properties [17]. Study methods typically attempt to enhance osteogenesis by applying a polarizing charge on a piezoelectric material under static conditions before placing the implant [18,19]. Some investigators have noted that the polarizing charge on a material is actually a result of ferroelectricity rather than a piezoelectric effect and that it can decay over time [20]. Alternatively, the

electroactivity of a piezoelectric material can be activated by mechanical forces [21]. Thus far, however, mechanical loading devices do not seem to be quantified, and safety concerns remain. Therefore, we aimed to find a more optimal method of mechanical loading.

Low-intensity pulsed ultrasound (LIPUS) is a non-invasive mechanical wave transmitted to the human body in the form of high-frequency pressure waves. Its unique advantages include non-invasiveness, efficacy, safety, ease of operation, and short treatment time. Since 1952, Corradi and others have used rabbit fracture models to confirm that LIPUS can accelerate callus formation. In 1983, studies confirmed that LIPUS has a therapeutic effect for bone healing on rabbits [22]. The US Food and Drug Administration approved LIPUS in 1994 as a clinical treatment for fresh fractures, delayed fracture healing, and nonunion fractures. A large number of studies have confirmed that LIPUS can treat fractures and promote bone healing [23,24].

In this study, the surface of a TC4 titanium alloy was coated with BT to form a BT/TC4 composite that was then activated by applying LIPUS. Its morphology, dielectric constant, piezoelectric properies, and electric properties stimulated with LIPUS were characterized, and MC3T3-E1 cells were used to evaluate its biological performance. We explored the effects of LIPUS-activated biomimetic electroactivity in BT/TC4 materials on MC3T3-E1 cells as well as its mechanism.

2. Methods

2.1. Preparation and characteristics of the BT coating

Medical TC4 disks, $\Phi 34.5 \times L$ 2 mm^3 in size (provided by Institute of Metal Research, Chinese Academy of Sciences, China), were used as substrates. They were first ground with 2000-grit abrasive paper then polished with diamond polishing paste impregnated onto a cloth. Finally, the disks were washed in acetone, ethanol, and distilled water for 15 min in each.

Potassium hydroxide (KOH, Analytically pure, Sinopharm Chemical Reagent Co., China) and barium hydroxide octahydrate (Ba(OH)$_2$·8H$_2$O, Analytically pure, Sinopharm Chemical Reagent Co., China) were dissolved in deionized water to prepare the hydrothermal solution (0.1 mol/L and 0.6 mol/L, respectively).

After transferring the solution to a Teflon-lined stainless steel autoclave, the disks were soaked in the solutions. Synthesis was conducted at 180 °C for 5 h, and the autoclave was allowed to cool to ambient temperature naturally. The disks were then ultrasonically rinsed with deionized water three to six times (until the rinse water reached neutral pH) and were then dried for 12 h in an oven at 100 °C.

An Inspect F50 scanning electron microscope (SEM; FEI Co., USA), employing energy-dispersive X-ray spectroscopy (EDS; X-Max; Oxford Instruments Co., Britain), was used to observe the surface and cross-section microscopy and element compositions of the formed coatings. An X'pert Pro X-ray diffractometer (XRD; PANalytical Co., Netherlands) was used to obtain phase information from the BT/TC4 samples.

An impedance analyzer was used at room temperature to measure dielectric performance across frequencies ranging from 1 Hz to 10^5 Hz. The poling electric field was 10 kV/cm.

Piezoelectric properties of the BT/TC4 materials were evaluated using anatomic force microscope (AFM, Asylum Research MFP-3D, USA) with a piezoresponse force microscopy (PFM, Bruker, Germany) module. The PFM images were collected and recorded using a Ti/Ir-coated Si cantilever (Olympus Electrilever, Germany) with a nominal 2 N/m spring constant and a free air resonance frequency of 70 kHz. A sequence of DC biases imposed by a small AC driving voltage was applied on the surface of the BT/TC4 materials, and the corresponding PFM phase and amplitude were measured. The corresponding piezoelectric vibration signal was detected to acquire the strain-electric field hysteresis loop and to further evaluate the effective piezoelectric coefficient d$_{33}$ of the BT coating.

Samples were also characterized electrically using an electrochemical workstation (CST500; Corrtest Instruments Co., China). Current was measured between the working electrode and a counter electrode through a zero-resistance ammeter before the test was carried out at room temperature. The test solution was phosphate-buffered saline (PBS). A saturated calomel electrode was used as the reference electrode, and a small-area platinum electrode was used as the counter electrode. The ultrasound probe was immersed in PBS approximately 5 cm from the sample. The BT/TC4 and TC4 disks were divided into three groups each: the continuous ultrasound group, the sham group, and the intermittent ultrasound group. The first received continuous ultrasound at a frequency of 1 MHz and an intensity of 30 mW/cm^2; the second was treated in the same manner, but with the ultrasound generator turned off; and the third received each treatment successively for alternating 1-min periods.

2.2. Cell culture and seeding

The mouse pre-osteoblast cell line MC3T3-E1 (passaese-16) was obtained from the Central Laboratory, School of Stomatology, China Medical University then cultured in α-minimum essential medium (α-MEM; Gibco, China) supplemented with 10% fetal bovine serum (FBS; Four-Seasons Green, China) in a humidified atmosphere of 5% CO$_2$ at 37 °C. The culture medium was refreshed every two days. Cells were seeded on sample surfaces in six-well plates, and 2 mL medium was added to each well. After the seeded samples were further incubated for 24 h, LIPUS stimulation was initiated.

The samples were randomly divided into four groups: BT/TC4 materials stimulated with LIPUS (UBT/TC4 group), TC4 materials stimulated with LIPUS (UTC4 group), BT/TC4 materials with sham stimulation (CBT/TC4 group), and TC4 materials with sham stimulation (CTC4 group).

2.3. LIPUS stimulation

Therapeutic LIPUS stimulation was applied to the samples using a Sonicator 740 (Mettler Electronics Corp., USA) with a plane-wave ultrasound transducer (ME7410; area of 10 cm^2), delivering an ultrasound wave comprising a sinusoidal ultrasound pulse 1 ms in length and 1 MHz in frequency, with a repetition rate of 100 Hz and a spatial average-temporal average intensity of 30 mW/cm^2. As shown in Fig. 1, the ultrasound probe was immersed in water approximately 5 cm from the sample. Daily exposure was 20 min. The sham group was treated likewise with the ultrasound generator turned off. These parameters were selected based on previous findings by our group [25–27].

2.4. Cell attachment and morphology

Morphology in the MC3T3-E1 cells on the sample surfaces was observed using SEM (S–3400 N; Hitachi, Japan) four days after seeding. Samples were rinsed three times in PBS and fixed overnight in 2.5% glutaraldehyde at 4 °C after which they were dehydrated through a graded ethanol series (60%–100%) then dried using the critical point method. After mounting them on studs, they were sputter-coated with gold/palladium then examined using SEM.

2.5. Wound-healing migration assay

Samples were cultured for 24 h, then a cell-free gap was created centrally using a pipette tip with a width of 1 mm. At specific time points (0, 1, and 3 days) after media removal, cells were fixed with 4% polyformaldehyde for 20 min then rinsed twice with PBS and stained with 4',6-diamidino-2-phenylindole fluorescent dye (DAPI; Beyotime Biotechnology, China) for 10 min. Stained samples were rinsed twice with PBS before inspection using fluorescence microscopy. Image analysis software (Image-Pro Plus 6.0; USA) was used to locate and evaluate the gap, and wound-healing rates were calculated based on
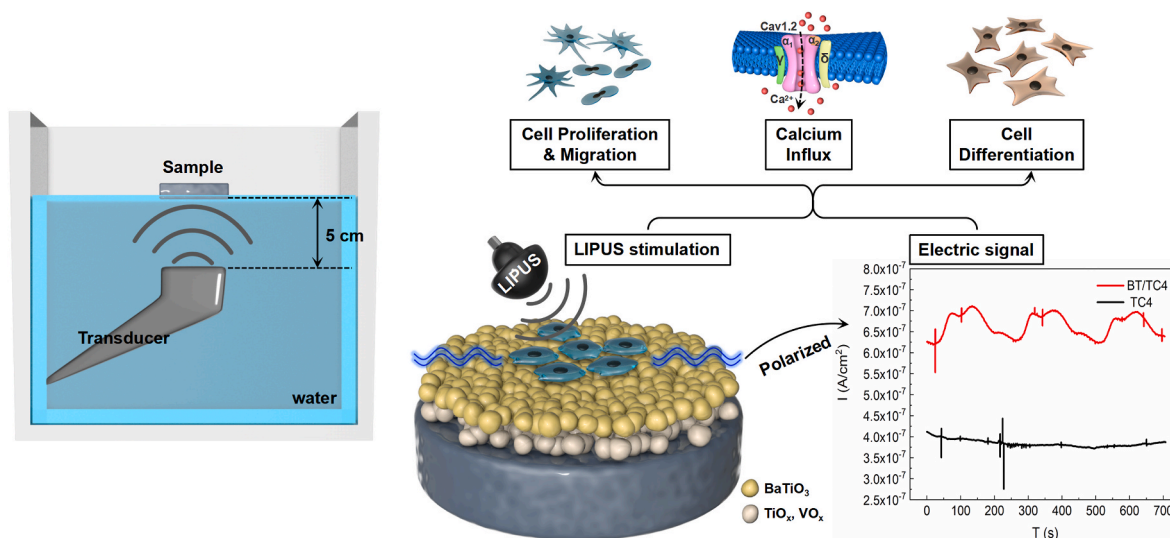
Fig. 1. A schematic diagram of LIPUS loading *in vitro* study.

wound closure, applying the following formula:

$$\text{Would healing rate } (\%) = 1 - \frac{\text{Gap area at indicated time point (1 or 3 d)}}{\text{Initial gap area (0 d)}} \times 100\%$$

2.6. Cell proliferation assay

Cell proliferation was evaluated using 3-(4,5-dimethylthiazol-2-yl)-2,5-diphenyl tetrazolium bromide (MTT; Sigma-Aldrich Co., USA) assays. After 1, 4, and 7 days incubation, the medium was removed and the cells were rinsed three times with PBS. To each well, 400 μL MTT and 1600 μL fresh α-MEM medium were added to each well and cultured for 4 h. The reaction was stopped by adding 2 mL dimethylsulfoxide, and the solution was transferred to new wells where absorbance was measured at 490 nm using an automatic microplate reader (Thermo-Fisher Co., USA).

2.7. Alkaline phosphatase activity assay

At days 1, 4, and 7, cells from various groups were rinsed three times with PBS then lysed with 0.3% Triton X-100. Lysates were briefly vortexed then centrifuged at 12,000 rpm for 5 min. The clear supernatant was used to measure alkaline phosphatase (ALP) activity, determined using an ALP activity assay kit. Total protein concentration in the supernatant was measured using a bicinchoninic acid protein assay kit (Jiancheng Co., China), and optical density (OD) was measured under a microplate reader at 520 nm. Finally, ALP activity was calculated using the following formula:

$$\text{ALP } (U / g \text{ prot}) = \frac{\frac{OD_{test} - OD_{blank}}{OD_{standard} - OD_{blank}} \times (\text{phenol content})_{standard}}{(\text{protein concentration})_{test}}$$

2.8. Osteocalcin content

After 7, 10, and 14 days of incubation, osteocalcin (OCN) secretion, as the release of extracellular matrix protein, was measured using a commercial OCN mouse enzyme-linked immunosorbent assay kit

(HuoLe Biotech, China), as described elsewhere [26].

2.9. Quantitative real-time polymerase chain reaction

Manufacturer instructions were followed to extract total RNA from the MC3T3-E1 cells using TRIzol (Trizol reagent, Sigma-Aldrich, USA). RNA concentrations were measured using a NanoDrop ND-2000 spectrophotometer at 260 nm. The RNA was reverse-transcribed using a reverse transcription system (Promega, Madison, WI). Quantitative real-time polymerase chain reaction (qRT-PCR) was performed using an ABI Prism 7500 RT-PCR system (Applied Biosystems, USA) using SYBR green fluorescence quantification. All primer sequences are shown in Supplementary Table S1.

2.10. Alizarin red staining

Mineralization of MC3T3-E1 cells was determined by alizarin red staining. On day 21, cells were washed twice with distilled water and fixed in 4% formalin for 30 min. Afterwards, cells were rinsed twice with deionized water and stained with 0.1% alizarin red (pH = 4.2, Soledad Bao Tech., China) for 30 min at room temperature. After staining, the excessive dye was gently washed with deionized water. Cells were de-stained for 30 min with 2 mL 10% hexadecylpyridinium chloride monohydrate (Sigma-Aldrich, USA) at room temperature. The eluates were transferred to the high-clarity polypropylene tubes to compare the color and exclude color interference caused by the background difference between BT/TC4 and TC4 materials. Finally, the OD values were measured at 550 nm using an enzyme-labelling instrument (Infinite M200, Switzerland).

2.11. Western blot

Cells were lysed in RIPA buffer (Beyotime Biotech., China), and the extracted protein was quantified using a bicinchoninic acid protein assay kit (Beyotime, Beijing, China). Protein samples were resolved using 10% sodium dodecyl sulfate-polyacrylamide gel electrophoresis,

transferring onto polyvinlyidene fluoride (PVDF) membranes and inhibiting with milk for 2 h at room temperature (5% w/v) in tris-buffered saline (TBS) with Tween-20 (0.1%; TBS-T). Blots were incubated with primary antibodies overnight at 4 °C and then with goat anti-rabbit horseradish peroxidase-conjugated secondary antibodies at 4 °C for 1 h then detected using an Enhanced Chemiluminescence Detection Kit (Boster, USA). All antibodies used are shown in Supplementary Table S2.

2.12. Intracellular calcium ion concentration

Intracellular calcium ion concentration was quantified via fluorescence microscopy aided with Fluo-4-AM (Dojindo, Japan). Cells cultured for 7 days were used to compare changes in calcium ion concentrations between groups. To determine whether opening of the L-type calcium channel played a major role in calcium ion changes in various groups, verapamil and SKF-96365 were used as inhibitors to the L-type calcium channels and stored calcium channels (SOCs), respectively.

Each of the four sample groups were further randomly divided into three groups: the blank group, the verapamil group, and the SKF-96365 group. The verapamil group was cultured in a complete medium containing 10 μmol/L verapamil (MCE, USA), whereas the SKF-96365 group was cultured in the complete medium containing 10 μmol/L SKF-96365 (MCE, USA). The blank group was cultured in the complete medium. After 24 h, each group was exposed to LIPUS or sham stimulation followed by calcium ion fluorescence staining.

Cells were rinsed twice with Hanks' balanced salt solution, incubated in the dark for 30 min at 37 °C in a culture medium containing Fluo-4-AM, then rinsed three more times with the salt solution. An inverted fluorescence microscope (FluoView1000; Olympus, Japan) was adapted to record emission fluorescence at an exaction wavelength of 494 nm and an emission wavelength of 533 nm. Fluorescence intensity was determined using image analysis software (Image-Pro Plus 6.0, USA).

2.13. Statistical analysis

SPSS 21.0 was used for statistical analyses. Results, expressed as means ± standard deviations (SDs), were verified using the Student *t*-test. Statistical significance was recognized at $P < 0.05$.

3. Results

3.1. Characterization results

3.1.1. Microstructure

Surface morphology of TC4 disks coated with BT is shown in Fig. 2A and B. While the surfaces were smooth, scratches from polishing remained. No cracks or spallation occurred in the BT coatings, and BT crystals, about 50 nm in size, were tightly bound together. Both Ba and Ti were identified on the BT/TC4 surface using EDS (Fig. 2D). As shown in Fig. 2C, a nanospheres-shaped coating being uniform in thickness of about 1.6 μm was formed on TC4 substrate. Combined with XRD spectrum shown in Fig. 2E, the elemental profiles of Ba, O and Ti, detected using EDS in cross-section of the coating, further confirmed that BT was present on TC4 substrate in a coating form.

3.1.2. Electric properties

Fig. 2F shows the dielectric constant curve for BT/TC4, indicating that it dropped rapidly between 0 and 100 Hz, then gradually stabilized as frequency increased. Between 100 and 10^5 Hz, the dielectric constant was 800–1000, a relatively high value for this application.

Fig. 2G shows the PFM topography obtained from the surface of the BT/TC4 material. Fig. 2H and I shows the PFM amplitude and phase of the BT/TC4 materials, respectively, demonstrating their piezoelectric behaviors. As shown in Fig. 2J and K, the displacement amplitude and

phase responses of the BT/TC4 materials exhibited butterfly loop, further confirming the ferroelectric nature of the BT/TC4 materials. The effective piezoelectric coefficient d_{33} was found using PFM to be about 0.42 pC/N.

The galvanic current varied in TC4 and BT/TC4 materials depending on ultrasound exposure, as shown in Fig. 2L-N. The BT/TC4 material generated a continuous and stable galvanic current of 60–65 μA/cm² when stimulated with ultrasound and 50–55 μA/cm² without it. This difference indicated that an additional galvanic current of approximately 10 μA/cm² was generated as a result of ultrasound stimulation. In the intermittent ultrasound group, galvanic current varied similarly: the peak-trough difference was approximately 10 μA/cm². Conversely, the uncoated TC4 substrate generated the same current (40–45 μA/cm²) with or without ultrasound stimulation and when the stimulation was intermittent.

3.2. Effects of materials/LIPUS on cellular biological behaviors

3.2.1. Cell adhesion, migration, and proliferation

After incubation for four days, SEM indicated that MC3T3-E1 cells adequately covered the surfaces in all groups. Cells exhibited a shuttle, polygonal shape with obvious pseudopods, and intercellular filaments could be seen. The UBT/TC4 group exhibited the greatest cell density in that cells covered nearly the entire sample surface.

On day 3, cell migration (healing rate) was greater in the UTC4 and CBT/TC4 groups than the CTC4 group ($P < 0.05$), and it was greater in the UBT/TC4 group than in the other three groups, pooled ($P < 0.05$).

On days 4 and 7, the MTT values were also greater in the UTC4 and CBT/TC4 groups than the CTC4 group (both $P < 0.05$), and it was also greater in the UBT/TC4 group than in the other three groups, pooled ($P < 0.05$). Fig. 3 illustrates these results.

3.2.2. Osteogenic differentiation in the cells

Using qRT-PCR and western blotting, the relative expressions of ALP, OCN/type I collagen (Col I), and Runx-2 were shown to be greater in the CBT/TC4 group compared to the CTC4 group ($P < 0.05$) at the mRNA and protein levels. Likewise, these expressions were greater in the UTC4 group compared to the CTC4 group ($P < 0.05$) and in the UBT/TC4 group compared to the other three groups, pooled ($P < 0.05$).

The ALP assays showed that ALP activity increased over time in every group. On days 4 and 7, ALP activity was greater in the CBT/TC4 and UTC4 groups compared to the CTC4 group (both $P < 0.05$). Additionally, it was greater in the UBT/TC4 group than the other three groups, pooled ($P < 0.05$).

The OCN content also increased over time in every group. On days 10, and 14, OCN content was greater in the UTC4 and CBT/TC4 groups compared to the CTC4 group (both $P < 0.05$). It was also greater in the UBT/TC4 group than the other three groups, pooled ($P < 0.05$).

The alizarin red staining assay on day 21 showed that the highly abundant mineralization nodules were showed in the UBT/TC4 group while only small mineralization foci in the CTC4 group, and the level of mineralization in UTC4 group and CBT/TC4 group were between that of the above two groups. The semiquantitative analysis of mineralization also showed the OD value was greater in the UTC4 and CBT/TC4 groups than the CTC4 group (both $P < 0.05$), and it was also greater in the UBT/TC4 group than in the other three groups, pooled ($P < 0.05$). Fig. 4 illustrates these results.

3.3. Changes in intracellular calcium ion concentration

3.3.1. Effect of material/LIPUS on intracellular calcium concentration

After either LIPUS or sham stimulation for seven days, intracellular calcium ion concentration was greater in the UTC4 and CBT/TC4 groups compared to the CTC4 group (both $P < 0.05$). It was also greater in the UBT/TC4 group than the other three groups, pooled ($P < 0.05$). Fig. 5A illustrates these results.
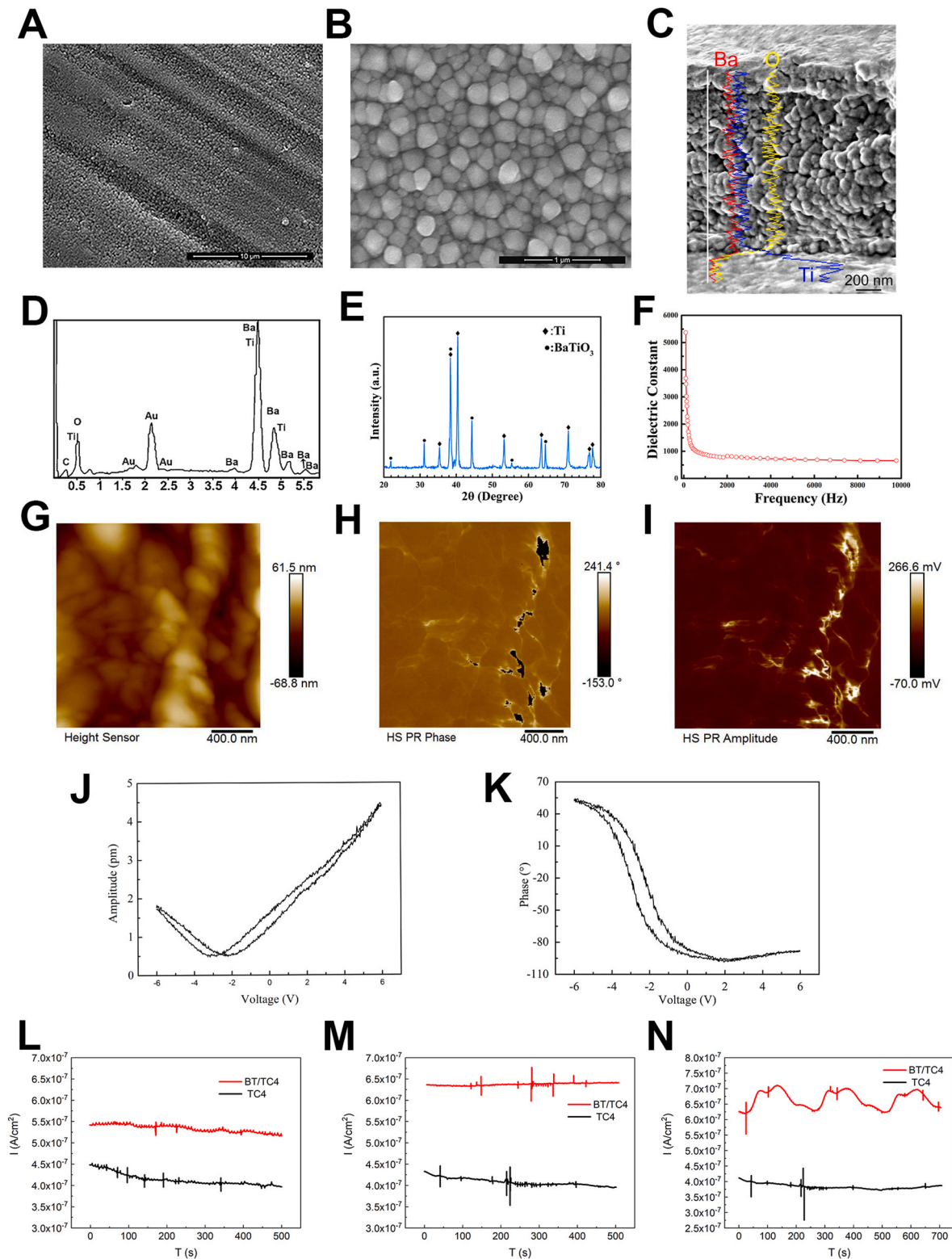
Fig. 2. Characterizations of BT coatings. (A) and (B) Surface SEM images of BT/TC4 materials. (C) Cross-section SEM image of BT/TC4 material, the morphology and elemental profiles of Ba, O and Ti. (D) EDS spectrum analysis of the BT coating. (E) XRD patterns of the BT coating. (F) Dielectric constant, ε', versus frequency for BT/TC4 material. (G) AFM topography. (H) PFM phase. (I) PFM amplitude. (J) Displacement amplitude and (K) phase of PFM switching at different locations using top electrode from electrical measurements. (L) Galvanic current of BT/TC4 and TC4 materials in sham group. (M) Galvanic current of BT/TC4 and TC4 materials exposed to continuous ultrasound. (N) Galvanic current of BT/TC4 and TC4 materials in intermittent ultrasound group.
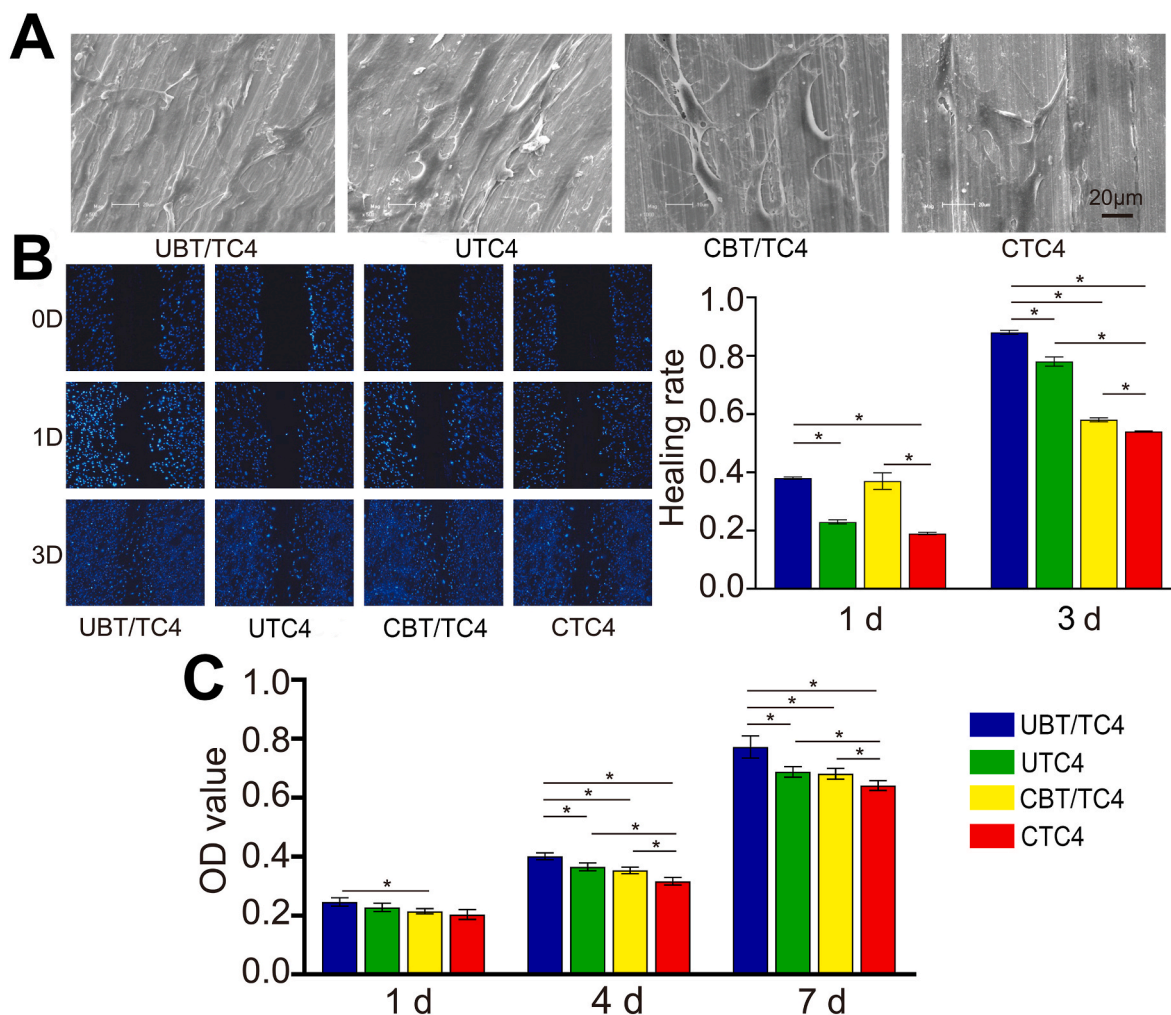
Fig. 3. Influences of material/LIPUS on cell behaviors include altered adhesion, migration, and proliferation. (A) SEM images of cell adhesion testing for MC3T3-E1 cells on day 4. (B) Results of wound healing migration assays on days 1 and 3. (C) MTT assay results on days 1, 4, and 7. LIPUS and BT/TC4 material increased cell migration and proliferation compared to the TC4 substrate without LIPUS. Combining the BT/TC4 material with LIPUS stimulation could further promote cell migration and proliferation of MC3T3-E1 cells, compared to either one alone. *$P < 0.05$.

3.3.2. Opening the L-type calcium channel regulates calcium in the cells on LIPUS-stimulated BT/TC4

Among the blanks, calcium ion concentration was greater in the UTC4 and CBT/TC4 groups compared to the CTC4 group (both $P < 0.05$). It was also greater in the UBT/TC4 group than the other three groups, pooled ($P < 0.05$). With the use of verapamil to inhibit opening of the L-type calcium channels, these differences became nonsignificant. However, with the use of SKF-96365 to inhibit the opening of SOCs, the differences remained. Fig. 5B illustrates these results.

3.3.3. Expression of the Ca$_V$1.2 protein in MC3T3-E1 cells

After seven days of incubation, the relative mRNA and protein expressions of the calcium channel protein Ca$_V$1.2 were greater in the UTC4 group compared to the CTC4 group ($P < 0.05$) and in the UBT/TC4 group compared to the other three groups, pooled ($P < 0.05$). The differences between the CBT/TC4 group and the CTC4 group were nonsignificant. Fig. 5C and D illustrate these results.

4. Discussion

The use of SEM, EDS, and XRD allowed the BT ceramic coating to be characterized, showing that it was successfully formed on the surface of the TC4 titanium alloy. PFM results suggested that BT/TC4 materials possessed piezoelectric behaviors. The d$_{33}$ of the BT coating (0.42 pC/N)

and of natural bone (up to 0.7 pC/N) were of the same order of magnitude, indicating that BT/TC4 materials could mimic the piezoelectric properties of bone, giving it a therapeutic potential for bone formation and remodeling under further mechanical forces [28]. Electrochemical measures indicated that an additional microcurrent of approximately 10 μA/cm^2 was generated when BT/TC4 was stimulated by ultrasound. This is direct evidence of electroactivity from the BT coating. Other researchers have shown electric-stimulated osteogenesis, adopting currents ranging from 5 to 50 μA/cm^2, a range that encompasses our results [29]. The piezoelectric contribution efficiency of piezoelectric materials is frequency dependent [30]. Therefore, we also evaluated the frequency responses of the BT/TC4 materials and measured response curves presented in the supplementary files. (Section S1 and Fig. S1). Further studies should be conducted to measure the magnitude and bioeffects of the microcurrent generated when different LIPUS parameters are applied or when the implant shape is different. Even though the microcurrent measured using PBS could not be equated to that in blood, the measured microcurrent in PBS is of great importance when elucidating the electrical environment in a dynamic *in vitro* setting.

Trends in *in vitro* experiments are similar, indicating that LIPUS as a mechanical stimulus can promote osteogenesis in MC3T3-E1 cells. When BT/TC4 material is stimulated with LIPUS, migration, proliferation, differentiation, and mineralization of MC3T3-E1 cells can be further
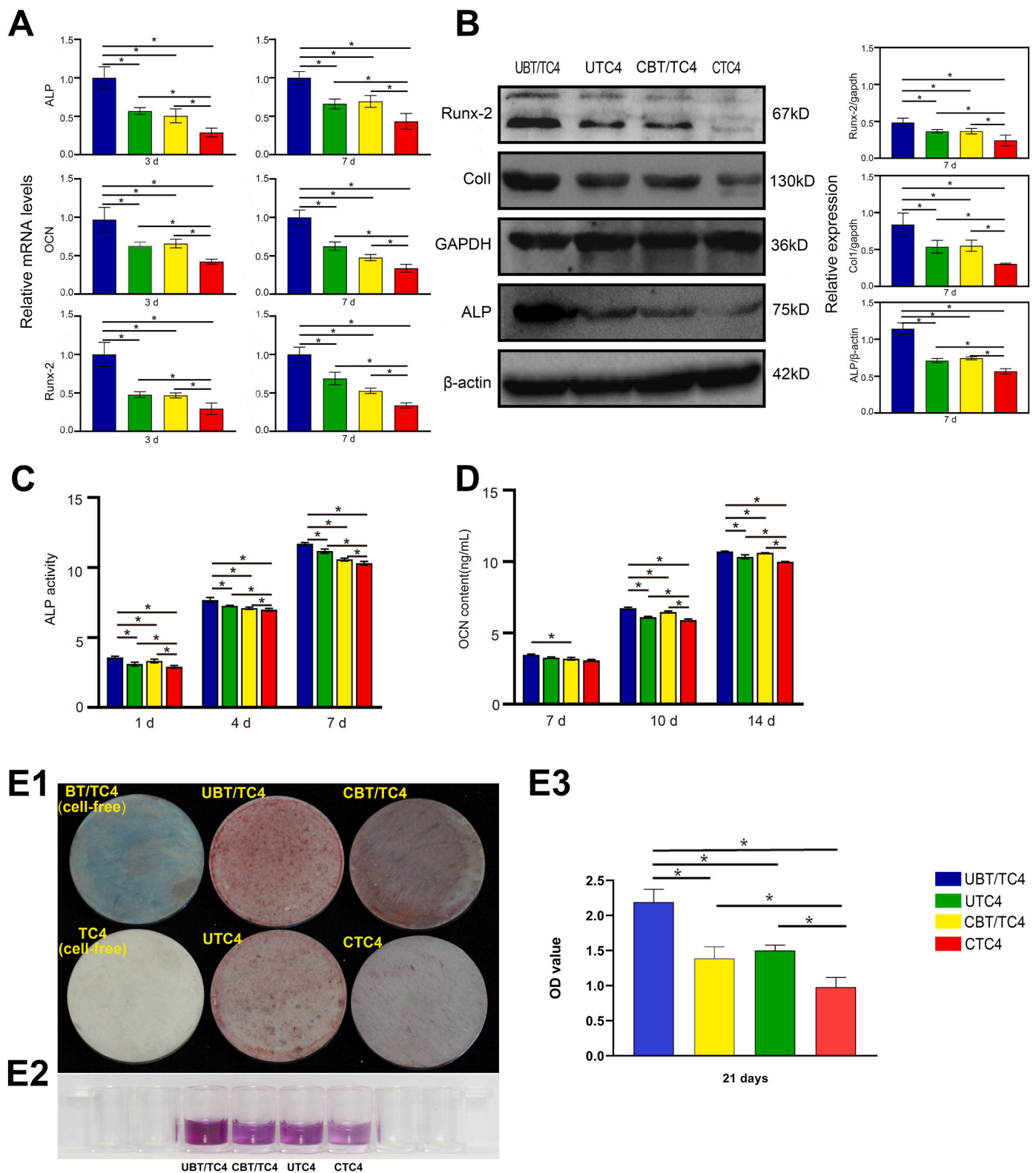
Fig. 4. Influences of material/LIPUS on osteogenic differentiation in MC3T3-E1 cells. (A) Quantitative real-time polymerase chain reaction was used to analyze the relative mRNA levels of ALP, Runx-2, and OCN on days 3 and 7. (B) Protein expression levels of ALP, type I collagen, and Runx-2 on day 7, determined using Western blot analysis. (C) ALP activity results on days 1, 4, and 7. (D) OCN enzyme-linked immunosorbent assay results on days 7, 10, and 14. (E1-E3) Alizarin red staining. (E1) General view. (E2) Eluates in the high-clarity polypropylene. (E3) Semiquantitative analysis of alizarin red staining. Individually, LIPUS and BT/TC4 materials increased osteogenic differentiation in MC3T3-E1 cells compared to the TC4 without LIPUS. Combining the BT/TC4 materials with LIPUS could further promote osteogenic differentiation in MC3T3-E1 cells compared to either one alone. *$P < 0.05$.
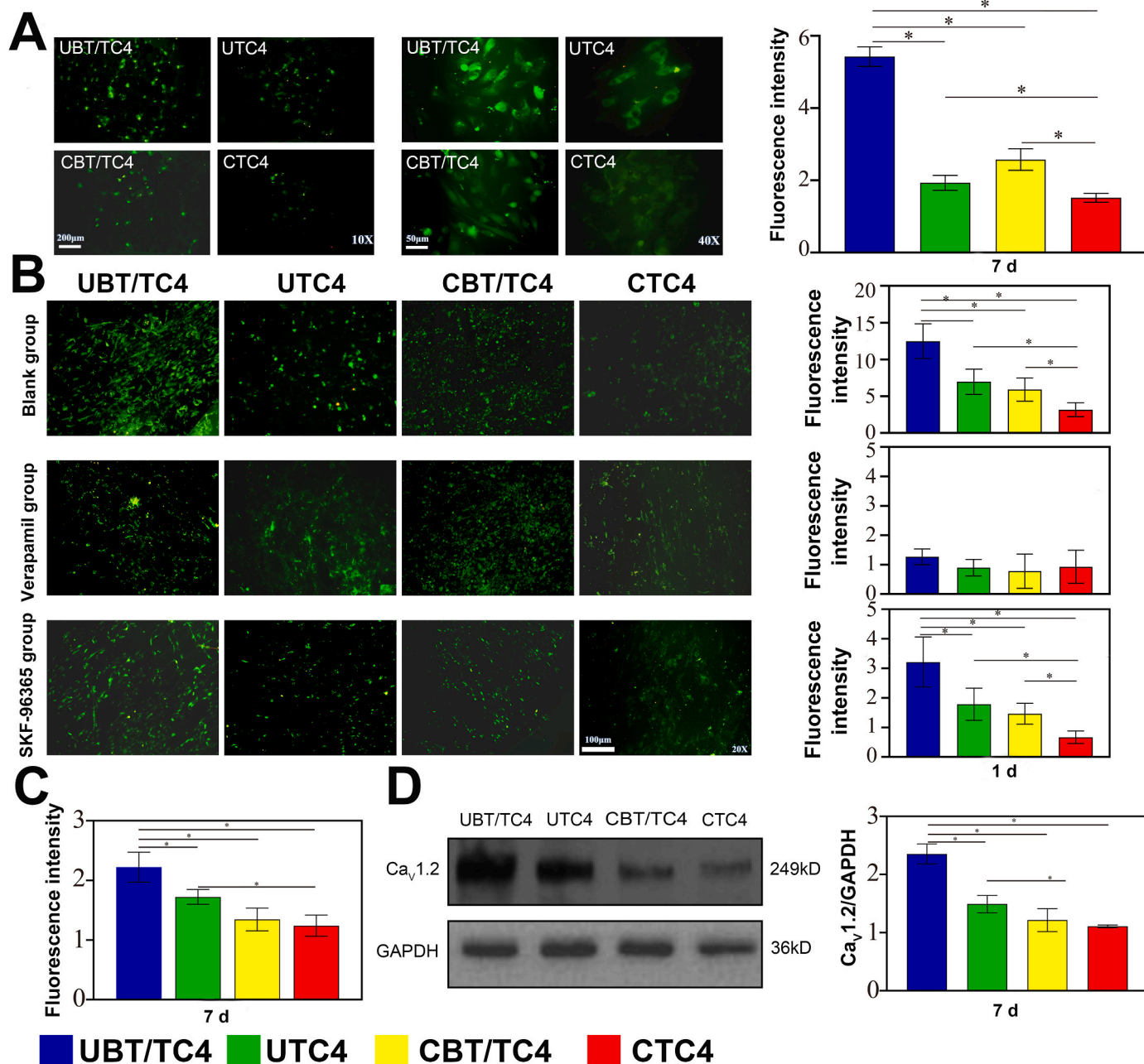
Fig. 5. Changes in intracellular calcium concentration in MC3T3-E1 cells depending on material, exposure to LIPUS, and the L-type calcium channel. (A) Intracellular calcium fluorescence staining in MC3T3-E1 cells on day 7 under various conditions. Individually, LIPUS and BT/TC4 material increased calcium ion concentrations in MC3T3-E1 cells. Combining the BT/TC4 materials with LIPUS stimulation could further promote the intracellular calcium ion concentrations in MC3T3-E1 cells. (B) Intracellular calcium fluorescence staining of MC3T3-E1 cells on day 1 in a blank and samples inhibited by verapamil or SKF-96365. (C) Relative $Ca_V1.2$ mRNA expression quantified using quantitative real-time polymerase chain reaction. (D) Western blot analysis to quantify calcium ion channel protein ($Ca_V1.2$) levels. *$P < 0.05$.

promoted. Some researchers report that the piezoelectric signal in bone has an apparent relaxation phenomenon: the piezoelectric voltage between electrodes cannot be maintained at steady state because the charges can be discharged through the bone tissue itself. In a static setting, it is difficult to maintain the charge at any given level [31]. Combination of piezoelectric materials with mechanical forces could simulate the piezoelectric effects in natural bone. Some studies have confirmed that piezoelectric implants activated by dynamically mechanical loading provided superior osteogenesis compared to those without mechanically loading [18,32]. Shuai used a different but similar loading device, showing that the ultrasound stimulation together with the BT/PVDF piezoelectric composite scaffold promoted differentiation in MG63 cells [33]. These methods of mechanical loading have not yet been applied in a clinical setting, and to do so requires further efforts to verify their efficacy and safety. The LIPUS used in our study provided an option for mechanical force loading on the piezoelectric materials that is not yet documented in the literature even though it has been approved by the U.S. FDA for the treatment of fresh fractures and existing non-union fractures. The parameters we applied were screened in earlier stages of research and were confirmed through both *in vivo* and *in vitro* biological experiments to promote osteogenesis in MC3T3-E1 cells [25–27]. Those parameters can be changed, allowing tissue-specific physiological demands to be fulfilled. Further studies would elucidate those specific parameters.

Intracellular calcium is a second messenger in cells, and it plays an important role in osteogenesis [34,35]. Studies have shown that the concentration of intracellular calcium ion is positively associated with adhesion, migration, proliferation, and differentiation in MC3T3-E1 cells via modulation of a large variety of intracellular downstream signal targets. For example, calcium-sensing receptor is able to functionally couple to integrins, in conjunction with facilitating intracellular calcium release, to promote cellular adhesion and migration [36]. The promoted calcium in MC3T3-E1 cells of G_0/G_1 phase is able to initiate the tricarboxylic acid cycle, which in turn activates downstream pathways involved in cell proliferation [37,38]. The promoted calcium also allows to facilitate osteogenic differentiation via the $Ca^{2+}/CaMKII/ERK/AP-1$ signaling pathway [39]. In addition, both mechanical and electrical stimulation can induce the promoted concentration of intracellular calcium ion influx [40,41]. Therefore, calcium influx may be a possible mechanism that is responsible for the promotion of osteogenesis of MC3T3-E1 cells on BT/TC4 materials stimulated with LIPUS.

Our calcium imaging results indicate that LIPUS can increase this concentration, and it was greatest in the UBT/TC4 group, indicating that electroactivity in BT/TC4, excited by LIPUS, was responsible for the increase. L-type calcium channels are voltage-dependent ion channels that play pivotal roles in regulating the free calcium concentration in living cells, affecting the intracellular calcium ion concentration by opening or closing the channels or by increasing or decreasing expression of the channels [42]. Our data show that blocking the L-type calcium channels using verapamil removes the differences in calcium ion concentrations among the groups, indicating that the L-type calcium channel is critical to the process. The other major calcium regulators are the SOCs, found primarily in the endoplasmic reticulum membrane [43]. Our data show that blocking the SOCs using SKF-96365 was not effective in removing the differences among the groups, suggesting that the SOCs might not be functional. The short time interval of one day was chosen to minimize the influence of calcium channel expression. The $Ca_V1.2$ protein represents the primary L-type calcium channel structural protein in MC3T3-E1 cells [44]. Some studies suggest that its expression is related to mechanical forces, consistent with our study [40,45]. Furthermore, electroactivity excited by LIPUS in BT/TC4 could further promote transcription and expression of the $Ca_V1.2$ protein. The piezoelectric effect might be another important reason for promoting calcium influx into MC3T3-E1 cells.

5. Conclusion

LIPUS-stimulated BT/TC4 has the ability to generate a piezoelectric signal which then enhances the osteogenic effects of MC3T3-E1 osteoblasts along with the influx of calcium ions, mediated by the L-type calcium channel. Combining a BT coating with LIPUS stimulation could be a potential method for forming early bone-implant contact in bone regeneration applications.

CRediT authorship contribution statement

Kunzhan Cai: Conceptualization, Investigation, Methodology, Writing – original draft. **Yilai Jiao:** Resources, Methodology, Formal analysis. **Quan Quan:** Methodology. **Yulin Hao:** Resources. **Jie Liu:** Resources. **Lin Wu:** Project administration, Funding acquisition, Supervision, Writing – review & editing.

Declaration of competing interest

The authors declare that they have no known competing financial interests or personal relationships that could have appeared to influence the work reported in this paper.

Acknowledgements

Appendix A. Supplementary data

Supplementary data to this article can be found online at https://doi.org/10.1016/j.bioactmat.2021.04.016.

References

[1] T. Takizawa, N. Nakayama, H. Haniu, K. Aoki, M. Okamoto, H. Nomura, M. Tanaka, A. Sobajima, K. Yoshida, T. Kamanaka, K. Ajima, A. Oishi, C. Kuroda, H. Ishida, S. Okano, S. Kobayashi, H. Kato, N. Saito, Titanium fiber plates for bone tissue repair, Adv. Mater. 30 (2018), https://doi.org/10.1002/adma.201703608.

[2] D. Silva, C. Guerra, H. Muñoz, C. Aguilar, M. Walter, M. Azocar, L. Muñoz, E. Gürbüz, A. Ringuedé, M. Cassir, M. Sancy, The effect of staphylococcus aureus on the electrochemical behavior of porous Ti-6Al-4V alloy, Bioelechem 136 (2020) 107622, https://doi.org/10.1016/j.bioelechem.2020.107622.

[3] M. Niinomi, Design and development of metallic biomaterials with biological and mechanical biocompatibility, J. Biomed. Mater. Res. 107 (2019) 944–954, https://doi.org/10.1002/jbm.a.36667.

[4] F.J. Aguilar-Pérez, R.F. Vargas-Coronado, J.M. Cervantes-Uc, J.V. Cauich-Rodríguez, R. Rosales-Ibañez, J.A. Rodríguez-Ortiz, Y. Torres-Hernández, Titanium-castor oil based polyurethane composite foams for bone tissue engineering, J. Biomater. Sci. Polym. Ed. 30 (2019) 1415–1432, https://doi.org/10.1080/09205063.2019.1636352.

[5] X. Rao, J. Yang, J. Li, X. Feng, Z. Chen, Y. Yuan, B. Yong, C. Chu, X. Tan, Q. Song, Replication and bioactivation of Ti-based alloy scaffold macroscopically identical to cancellous bone from polymeric template with TiNbZr powders, J Mech Behav Biomed Mater 88 (2018) 296–304, https://doi.org/10.1016/j.jmbbm.2018.08.031.

[6] D. Oltean-Dan, G.B. Dogaru, M. Tomoaia-Cotisel, D. Apostu, A. Mester, H.R. Benea, M.G. Paiusan, E.M. Jianu, A. Mocanu, R. Balint, C.O. Popa, C. Berce, G.I. Bodizs, A. M. Toader, G. Tomoaia, Enhancement of bone consolidation using high-frequency pulsed electromagnetic short-waves and titanium implants coated with biomimetic composite embedded into PLA matrix: in vivo evaluation, Int. J. Nanomed. 14 (2019) 5799–5816, https://doi.org/10.2147/IJN.S205880.

[7] N. Jiang, Z. Guo, D. Sun, Y. Li, Y. Yang, C. Chen, L. Zhang, S. Zhu, Promoting osseointegration of Ti Implants through micro/nanoscaled hierarchical Ti phosphate/Ti oxide hybrid coating, ACS Nano 12 (2018) 7883–7891, https://doi.org/10.1021/acsnano.8b02227.

[8] S.A. Aleksandrova, O.I. Aleksandrova, V.P. Khomutov, M.S. Morgunov, M. I. Blinova, The influence of an electret-generated electric field based on a tantalum oxide anode on differentiation properties of bone marrow stromal cells from patients with osteoarthritis, Cell and Tissue Biology 13 (2019) 144–151, https://doi.org/10.1134/S1990519X19020020.

[9] F. Vasquez-Sancho, A. Abdollahi, D. Damjanovic, G. Catalan, Flexoelectricity in bones, Adv. Mater. 30 (2018), https://doi.org/10.1002/adma.201705316.

[10] A.H. Rajabi, M. Jaffe, T.L. Arinzeh, Piezoelectric materials for tissue regeneration: a review, Acta Biomater. 24 (2015) 12–23, https://doi.org/10.1016/j.actbio.2015.07.010.

[11] C.K. Jeong, Toward bioimplantable and biocompatible flexible energy harvesters using piezoelectric ceramic materials, MRS Commu 10 (2020) 365–378, https://doi.org/10.1557/mrc.2020.48.

[12] J.B. Park, B.J. Kelly, G.H. Kenner, A.F. von Recum, M.F. Grether, W.W. Coffeen, Piezoelectric ceramic implants: in vivo results, J. Biomed. Mater. Res. 15 (1981) 103–110, https://doi.org/10.1002/jbm.820150114.

[13] A.K. Dubey, G. Thrivikraman, B. Basu, Absence of systemic toxicity in mouse model towards BaTiO3 nanoparticulate based eluate treatment, J. Mater. Sci. Mater. Med. 26 (2015) 103, https://doi.org/10.1007/s10856-015-5414-6.

[14] I. Chae, C.K. Jeong, Z. Ounaies, S.H. Kim, Review on electromechanical coupling properties of biomaterials, ACS Appl. Bio Mater. 1 (2018) 936–953, https://doi.org/10.1021/acsabm.8b00309.

[15] B. Liu, L. Chen, C. Shao, F. Zhang, K. Zhou, J. Cao, D. Zhang, Improved osteoblasts growth on osteomimetic hydroxyapatite/BaTiO3 composites with aligned lamellar

porous structure, Mater Sci Eng C Mater Biol Appl 61 (2016) 8–14, https://doi.org/10.1016/j.msec.2015.12.009.

[16] X. Zhang, C. Zhang, Y. Lin, P. Hu, Y. Shen, K. Wang, S. Meng, Y. Chai, X. Dai, X. Liu, Y. Liu, X. Mo, C. Cao, S. Li, X. Deng, L. Chen, Nanocomposite membranes enhance bone regeneration through restoring physiological electric microenvironment, ACS Nano 10 (2016) 7279–7286, https://doi.org/10.1021/acsnano.6b02247.

[17] M.M. Alvarez, J. Aizenberg, M. Analoui, A.M. Andrews, G. Bisker, E.S. Boyden, R. D. Kamm, J.M. Karp, D.J. Mooney, R. Oklu, D. Peer, M. Stolzoff, M.S. Strano, S. G. Trujillo-de, T.J. Webster, P.S. Weiss, A. Khademhosseini, Emerging trends in micro and nanoscale technologies in medicine: from basic discoveries to translation, ACS Nano 11 (2017) 5195–5214, https://doi.org/10.1021/acsnano.7b01493.

[18] Y. Li, X. Dai, Y. Bai, Y. Liu, Y. Wang, O. Liu, F. Yan, Z. Tang, X. Zhang, X. Deng, Electroactive BaTiO$_3$ nanoparticle-functionalized fibrous scaffolds enhance osteogenic differentiation of mesenchymal stem cells, Int. J. Nanomed. 12 (2017) 4007–4018, https://doi.org/10.2147/IJN.S135605.

[19] Y. Tang, C. Wu, Z. Wu, L. Hu, W. Zhang, K. Zhao, Fabrication and *in vitro* biological properties of piezoelectric bioceramics for bone regeneration, Sci. Rep. 7 (2017) 43360, https://doi.org/10.1038/srep43360.

[20] A. Ehterami, M. Kazemi, B. Nazari, P. Saraeian, M. Azami, Fabrication and characterization of highly porous barium titanate based scaffold coated by gel/HA nanocomposite with high piezoelectric coefficient for bone tissue engineering applications, J Mech Behav Biomed Mater 79 (2018) 195–202, https://doi.org/10.1016/j.jmbbm.2017.12.034.

[21] B. Tandon, J.J. Blaker, S.H. Cartmell, Piezoelectric materials as stimulatory biomedical materials and scaffolds for bone repair, Acta Biomater. 73 (2018) 1–20, https://doi.org/10.1016/j.actbio.2018.04.026.

[22] L.R. Duarte, The stimulation of bone growth by ultrasound, Arch. Orthop. Trauma Surg. 101 (3) (1983) 153–159, https://doi.org/10.1007/BF00436764.

[23] J. Liu, X. Li, D. Zhang, J. Jiao, L. Wu, F. Hao, Y.X. Qin, Acceleration of bone defect healing and regeneration by low-Intensity ultrasound radiation force in a rat tibial model, Ultrasound Med. Biol. 44 (2018) 2646–2654, https://doi.org/10.1016/j.ultrasmedbio.2018.08.002.

[24] X. Liu, Y. Hu, L. Wu, S. Li, Effects of collimated and focused low-intensity pulsed ultrasound stimulation on the mandible repair in rabbits, Ann. Transl. Med. 8 (2020) 98, https://doi.org/10.21037/atm.2019.12.89.

[25] L. Wu, L. Lin, Y. Qin, Enhancement of cell ingrowth, proliferation, and early differentiation in a three-dimensional silicon carbide scaffold using low-intensity pulsed ultrasound, Tissue Eng. 21 (2015) 53–61, https://doi.org/10.1089/ten.TEA.2013.0597.

[26] H. Cao, L. Feng, Z. Wu, W. Hou, S. Li, Y. Hao, L. Wu, Effect of low-intensity pulsed ultrasound on the biological behavior of osteoblasts on porous titanium alloy scaffolds: an *in vitro* and *in vivo* study, Mater Sci Eng C Mater Biol Appl 80 (2017) 7–17, https://doi.org/10.1016/j.msec.2017.05.078.

[27] L. Feng, X. Liu, H. Cao, L. Qin, W. Hou, L. Wu, A comparison of 1- and 3.2-MHz low-intensity pulsed ultrasound on osteogenesis on porous titanium alloy scaffolds: an *in vitro* and *in vivo* study, J. Ultrasound Med. 38 (2019) 191–202, https://doi.org/10.1002/jum.14683.

[28] Y. Zhang, L. Chen, J. Zeng, K. Zhou, D. Zhang, Aligned porous barium titanate/hydroxyapatite composites with high piezoelectric coefficients for bone tissue engineering, Mater Sci Eng C Mater Biol Appl 39 (2014) 143–149, https://doi.org/10.1016/j.msec.2014.02.022.

[29] R.A. Gittens, R. Olivares-Navarrete, R. Tannenbaum, B.D. Boyan, Z. Schwartz, Electrical implications of corrosion for osseointegration of titanium implants, J. Dent. Res. 90 (2011) 1389–1397, https://doi.org/10.1177/0022034511408428.

[30] A.S. B Edda R, P.D. Higgins, Use of ferroelectric-crystal detectors for electron dosimetry, IEEE Trans. Son. Ultrason. 37 (1990) 26–29, https://doi.org/10.1109/58.46966.

[31] Z. Hou, D. Fu, Q.H. Qin, An exponential law for stretching–relaxation properties of bone piezovoltages, Int.J Solids Struct. 48 (2011) 603–610, https://doi.org/10.1016/j.ijsolstr.2010.10.024.

[32] C. Ribeiro, J. Pärssinen, V. Sencadas, V. Correia, S. Miettinen, V.P. Hytönen, S. Lanceros-Méndez, Dynamic piezoelectric stimulation enhances osteogenic differentiation of human adipose stem cells, J. Biomed. Mater. Res. 103 (2015) 2172–2175, https://doi.org/10.1002/jbm.a.35368.

[33] C. Shuai, G. Liu, Y. Yang, W. Yang, C. He, G. Wang, Z. Liu, F. Qi, S. Peng, Functionalized BaTiO$_3$ enhances piezoelectric effect towards cell response of bone scaffold, Colloids Surf. B Biointerfaces 185 (2020) 110587, https://doi.org/10.1016/j.colsurfb.2019.110587.

[34] M. Zayzafoon, Calcium/calmodulin signaling controls osteoblast growth and differentiation, J. Cell. Biochem. 97 (2006) 56–70, https://doi.org/10.1002/jcb.20675.

[35] S. Wang, S. Li, M. Hu, B. Huo, Calcium response in bone cells at different osteogenic stages under unidirectional or oscillatory flow, Biomicrofluidics 13 (2019) 64117, https://doi.org/10.1063/1.5128696.

[36] S. Tharmalingam, A.M. Daulat, J.E. Antflick, S.M. Ahmed, E.F. Nemeth, S. Angers, A.D. Conigrave, D.R. Hampson, Calcium-sensing receptor modulates cell adhesion and migration via integrins, J. Biol. Chem. 286 (2011) 40922–40933, https://doi.org/10.1074/jbc.M111.265454.

[37] L. Yu, X. Wang, X. Gao, J. Tong, J. Zhang, The calcium transient characteristics induced by fluid shear stress affect the osteoblast proliferation, Exp. Cell Res. 362 (2018) 51–62, https://doi.org/10.1016/j.yexcr.2017.11.001.

[38] J. Tong, Y. Qi, X. Wang, L. Yu, C. Su, W. Xie, J. Zhang, Cell micropatterning reveals the modulatory effect of cell shape on proliferation through intracellular calcium transients, BBA-Mol Cell Res. 1864 (2017) 2389–2401, https://doi.org/10.1016/j.bbamcr.2017.09.015.

[39] M.K. Shin, M. Kim, Y. Bae, I. Jo, S. Lee, C. Chung, Y. Park, D.S. Min, A novel collagen-binding peptide promotes osteogenic differentiation via Ca^{2+}/calmodulin-dependent protein kinase II/ERK/AP-1 signaling pathway in human bone marrow-derived mesenchymal stem cells, Cell. Signal. 20 (2008) 613–624, https://doi.org/10.1016/j.cellsig.2007.11.012.

[40] N. Tsuchiya, D. Kodama, S. Goto, A. Togari, Shear stress-induced Ca^{2+} elevation is mediated by autocrine-acting glutamate in osteoblastic MC3T3-E1 cells, J. Pharmacol. Sci. 127 (2015) 311–318, https://doi.org/10.1016/j.jphs.2015.01.005.

[41] C.T. Brighton, W. Wang, R. Seldes, G.H. Zhang, S.R. Pollack, Signal transduction in electrically stimulated bone cells, J Bone Joint Surg AMJ 83 (2001) 1514–1523, https://doi.org/10.1177/10668690100900418.

[42] L. Wen, Y. Wang, H. Wang, L. Kong, L. Zhang, X. Chen, Y. Ding, L-type calcium channels play a crucial role in the proliferation and osteogenic differentiation of bone marrow mesenchymal stem cells, Biochem. Biophys. Res. Commun. 424 (2012) 439–445, https://doi.org/10.1016/j.bbrc.2012.06.128.

[43] L.J. Robinson, H.C. Blair, J.B. Barnett, M. Zaidi, C.L. Huang, Regulation of bone turnover by calcium-regulated calcium channels, Ann. N. Y. Acad. Sci. 1192 (2010) 351–357, https://doi.org/10.1111/j.1749-6632.2009.05219.x.

[44] F. Hofmann, V. Flockerzi, S. Kahl, J.W. Wegener, L-type Ca$_V$1.2 calcium channels: from *in vitro* findings to *in vivo* function, Physiol. Rev. 94 (2014) 303–326, https://doi.org/10.1152/physrev.00016.2013.

[45] J. Zuo, J. Zhen, F. Wang, Y. Li, Z. Zhou, Effect of low-intensity pulsed ultrasound on the expression of calcium ion transport-related proteins during tertiary dentin formation, Ultrasound Med. Biol. 44 (2018) 223–233, https://doi.org/10.1016/j.ultrasmedbio.2017.09.006.